Optical and Structural Properties of a Eu(II)-Doped Silico-aluminate with Channel Structure and Partial Site Occupation

Andreas Rief[a], Frank Kubel[a], and Hans Hagemann[b]

[a] Institute of Chemical Technologies and Analytics, Vienna University of Technology, Getreidemarkt 9/164-SC, A-1060 Vienna, Austria
[b] Dépt. de Chimie Physique, University of Geneva, 30, quai Ernest-Ansermet, CH-1211 Geneva 4, Switzerland

Reprint requests to Dr. A. Rief. E-mail: andreas.rief@tuwien.ac.at

Z. Naturforsch. **2007**, *62b,* 1535 – 1542; received June 14, 2007

A new barium silico-aluminate phase with the stoichiometry $Ba_{13.35(1)}Al_{30.7}Si_{5.3}O_{70}$ has been found and characterized. The compound crystallizes in the space group $P6_3/m$ (No. 176) with a = 15.1683(17), c = 8.8708(6) Å, V = 1767.5(4) Å^3, Z = 1, R_w = 0.026, 32 refined parameters. A 3-dimensional matrix of Al/SiO_4 tetrahedra with Ba(II) ions located in channels along the c axis builds up the structure. One of these channels is partially filled with Ba(II) ions (CN 6+3) in Wyckoff position 2a, leaving $\sim$ 1/3 of the positions empty. The second and third type of Ba(II) ions occupy channels orientated along the c axis with CN 4+2+2 and 4+3+1, respectively. The structure shows a rare clustered arrangement of six tetrahedra filled exclusively by Al(III) and therefore is an exception to Loewenstein's rule. The other tetrahedral positions show an Al to Si ratio of $\sim 4:1$. The Al/Si–O bond lengths in the tetrahedral Al/Si positions drawn *vs.* site occupation show linear behavior similar to the prediction by Vegard's rule for solid solutions. After doping with Eu(II) the compound shows bright orange-yellow luminescence with an unusual large shift of the Eu(II) emission band.

Key words: Disorder, Structure Refinement, Silico-aluminate, Luminescence, Channel Structure

Introduction

Alkaline earth silicates and aluminates can be used as host structures for rare earth elements to study optical properties such as fluorescence and phosphorescence. Only a limited number of compounds in the Al-rich Ba/Al/Si-O system are known and have been structurally characterized. Mainly the mineral celsian, $BaAl_2Si_2O_8$, as monoclinic (paracelsian) or as hexagonal modification (hexacelsian), was studied [1 – 3]. Synthetically grown silico-aluminates include a phase with a suggested composition $Ba_{13}Al_{22}Si_{10}O_{66}$ [4], a cubic barium zeolite $Ba_{46}Al_{92}Si_{100}O_{384}$ [5] and $Ba_3Al_2Si_3O_{12}$ [6]. Searching for new host materials for luminescent centers we tried to synthesize $Ba_{13}Al_{22}Si_{10}O_{66}$ as a new host for rare earth elements. Instead of the compound with the suggested formula a new phase was found in small yield. To obtain more information on the composition, crystal structure and formation of this silico-aluminate phase, single crystals were grown and studied.

Different ways to obtain single crystals of the compound by melting at high temperature were considered. If it is not practicable to grow single crystals out of a melt, because *e. g.* melting temperatures are too high, or aggressive melts are formed, the method of local flux growth is a way to obtain small crystals. A high-temperature molten salt, as *e. g.*, B_2O_3, PbF_2, NaCl, can be used to dissolve silicates or aluminates and to reduce thereby the melting point of the system. Adding only a small amount of a flux ($<$ 10 wt.-% for B_2O_3 acting like a mineralizer) favors liquid phase sintering in local areas only and allows using corundum crucibles for alumo-silicate and silico-aluminate synthesis instead of carbon crucibles in an inert gas atmosphere. Higher amounts of solvent form molten samples and result in destruction and reaction with the corundum crucible. Using this method, crystals suitable for X-ray structure analysis can be obtained at temperatures far lower than the melting point of the substrate. We were able to grow single crystals of the title compound and finally refined its structure from single crystal data as $Ba_{13.35(1)}Al_{30.7}Si_{5.3}O_{70}$ (abbreviated further on as BAS).

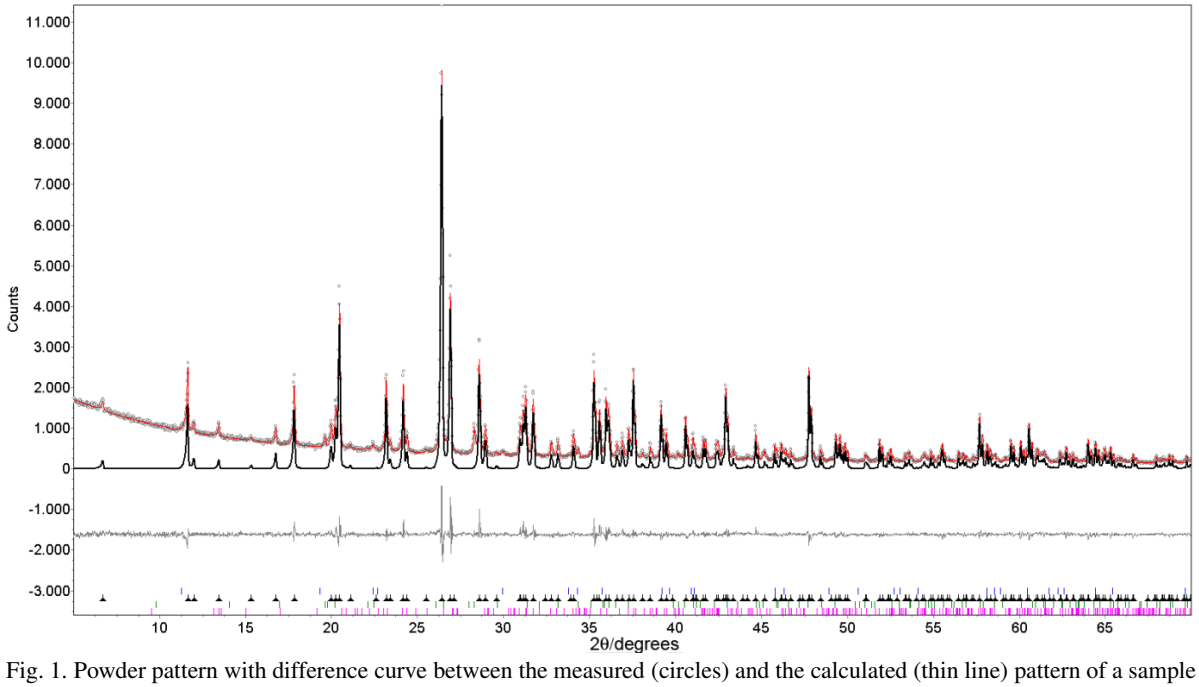

Fig. 1. Powder pattern with difference curve between the measured (circles) and the calculated (thin line) pattern of a sample including BAS (thick line) and $BaAl_2O_4$ and $BaAl_2Si_2O_4$ as by-phases. Triangles indicate calculated BAS signals.

Experimental Section

Synthesis

Colorless single crystals of BAS were synthesized from a carefully prepared mixture of pro analysis grade $BaCO_3$ (Merck), $Al(OH)_3$ (Merck) and SiO_2 (Fluka) with a 10 wt.-% addition of H_3BO_3 (Aldrich) as B_2O_3 source (H_3BO_3 dehydrates to B_2O_3 at $\sim$ 480 °C). The homogenized powder was pressed to pellets and fired at 1450 °C in a corundum crucible for 12 h. After firing, samples were cooled down to r. t. with a cooling rate of 180 °C h^{-1}. Under a polarized-light microscope, homogeneous fragments of the crushed sample showed sharp extinctions. They were separated and used for single crystal measurements.

Polycrystalline samples containing mainly BAS (96 wt.-%) with celsian and hexacelsian as by-products were synthesized from the same educts (but without H_3BO_3) as used for single crystal growth. Doping of BAS was carried out by adding small amounts (0.1 wt.-% Eu) of EuF_3 (Fluka) to the powder mixture. Firing was executed several times for 12 h at 1625 °C in corundum crucibles with intermediate grinding and pelleting. To compare yield and influence of the mineralizer, powder samples were also prepared with H_3BO_3 at 1450 °C. Reduction of the trivalent Eu doped powders was carried out in pure H_2 atmosphere for 2 h at 1000 °C.

Luminescence experiments

Luminescence experiments were performed at r. t. on powdered samples using a Jobin Yvon Fluorolog 3-22 instrument.

X-Ray diffraction analyses

Powder diffraction

Powder patterns were collected on a Phillips XPERT Bragg Brentano diffractometer. Rietveld refinement was carried out using the fundamental parameter approach with the TOPAS [7] software. Fig. 1 shows the powder pattern of a sample containing small amounts of hexagonal $BaAl_2Si_2O_8$ and $BaAl_2O_4$. Using the data from the single crystal measurements (see below) the powder pattern could be indexed and the phase composition refined. The main phase was BAS with 96(1) wt.-% of BAS; the remaining phases were $BaAl_2O_4$ (3(1) wt.-%) and hexacelsian (1(1) wt.-%). Lattice parameters of the polycrystalline BAS sample are a = 15.1776(3), c = 8.8705(2) Å and V = 1769.63(9) $Å^3$. Lattice parameters of BAS were determined on a sample containing 84 wt.-% BAS with Si (a = 5.4309 Å) as internal standard. Data collection and refinement parameters are summarized in Table 1.

Powder samples prepared in the presence of H_3BO_3 showed no difference in the lattice parameters larger than 3 σ as compared to the single crystal values, but partial substi-

Table 1. Data collection and refinement parameters of BAS (powder diffraction and single crystal data; e.s.d.'s in parentheses).

	Powder diffraction data	Single crystal data
Formula	$Ba_{13.35(1)}Al_{30.7}Si_{5.3}O_{70}$	
Formula weight, g mol^{-1}	3931(2)	3930.3(2)
Crystallite size, nm / Crystal size, mm^3	525(19)	$0.04 \times 0.03 \times 0.02$
Crystal system / space group	hexagonal / $P6_3/m$ (No. 176)	
a, Å	15.1776(3)	15.1683(17)
c, Å	8.8705(2)	8.8708(6)
V, Å^3	1769.63(9)	1767.5(4)
Z	1	1
Density, g cm^{-1}	3.68	3.68
Absorption coefficient μ, mm^{-1}	3.10	7.9
Temperature, K	295	293
Diffractometer type	Phillips XPERT	Enraf Nonius CAD4
Geometry	Bragg Brentano	Kappa
Detector	Phillips X'Celerator area det.	Scintillation counter
Radiation; wavelength, Å	Cu$K_{\alpha 1}$; 1.5406	MoK_α; 0.71073
Monochromator	graphite	graphite
θ Range, deg	5 – 70	2.7 – 39.9
Scan	–	ω
Scan speed, deg s^{-1}	0.01	0.09
Time per step, s	2.00	–
Step size, deg	0.020	–
Absorption correction	–	numerical
T_{min} / T_{max}	–	0.747 / 0.771
n_{ref} measured	283	4117
n_{ref} independent	283	3818
R_{int}	–	0.059
n_{ref} with $I \geq 3\sigma(I)$		1862
Number of refined parameters	7	32
Gof		1.41
R values	$R_{Bragg} = 0.065$	$R = 0.041$
	$R_{wp} = 0.074$	$R_w = 0.026$
$\Delta\rho_{min\,/\,max}$, e Å^{-3}		−5.1 / 5.7
Program used	TOPAS 2.0 [7]	XTAL 3.2

Table 2. Lattice parameters and site occupancy factors resulting from powder and single crystal refinements.

	Powder sample			Single crystal
	I (with boron)	II	III	
a, Å	15.1689(5)	15.1776(3)	15.1725(5)	15.1683(17)
c, Å	8.8780(4)	8.8705(2)	8.8834(3)	8.8708(6)
V, Å^3	1769.09(14)	1769.63(9)	1771.03(13)	1767.5(4)
SOF (Ba(2))	0.767(19)	0.677(7)	0.665(7)	0.667(2)
R values	$R_{Bragg} = 0.083$	$R_{Bragg} = 0.065$	$R_{Bragg} = 0.049$	$R = 0.041$
	$R_{wp} = 0.138$	$R_{wp} = 0.074$	$R_{wp} = 0.063$	$R_w = 0.026$

tution of Al by B, especially in the single crystal synthesis, cannot be excluded (Table 2). In the literature it has been reported for some systems that boron can occupy the Al positions [8]. For the title compound, substitution of Al by B did not improve the refinement. In addition, the lattice parameters of the single crystals in comparison with the powder data did not indicate any substantial boron substitution. Lattice constants of powder samples prepared with and without boron are in the same range as the single crystal data. Single phase polycrystalline samples were not obtained so far.

Single crystal diffraction

Crystals for single crystal diffraction were selected from a sample with 66(1) wt.-% BAS (Rietveld refinement with TOPAS from a powder pattern). By-phases in this mixture were $BaAl_2O_4$, $BaAl_2Si_2O_8$ and a small amount of quartz. Single crystal measurements were made on an Enraf Nonius CAD 4 diffractometer with a scintillation counter. Refinement of the BAS structure was done with XTAL 3.7 [9] and converged at $R_w = 2.6\,\%$. The compound crystallizes in the hexagonal space group $P6_3/m$ [176] with lattice parameters a = 15.1683(17) and c = 8.8708(6) Å, V = 1767.5(4) Å^3. Compared with the powder data, the lattice parameters are in the same range. No superstructure reflections were found in the powder patterns and the single crystal measurements. Data collection and refinement parameters are summarized in Table 1.

The structure was solved by locating the heavy atoms by Patterson Methods using a routine of the XTAL 3.7 package.

Table 3. Atomic positional parameters and site occupation factors for BAS.

Atom	*x*	*y*	*z*	SOF (Ba(2))
Ba(1)	0.33516(2)	0.25776(2)	1/4	
Ba(2)	0	0	1/4	0.667(2)
Ba(3)	0.43471(3)	0.39143(3)	3/4	
Al(1)	0.56824(8)	0.36681(8)	0.43148(11)	
Al(2)	0.20450(7)	0.01848(7)	0.43020(11)	0.779[a]
Si(2)	0.20450(7)	0.01848(7)	0.43020(11)	0.221[a]
Al(3)	0.28240(7)	0.42824(7)	0.43314(11)	0.779[a]
Si(3)	0.28240(7)	0.42824(7)	0.43314(11)	0.221[a]
O(1)	0.45629(17)	0.26355(19)	0.0005(3)	
O(2)	0.27896(19)	0.32872(19)	0.9673(3)	
O(3)	0.1925(2)	0.12526(18)	0.0602(3)	
O(4)	0.40212(17)	0.53032(18)	0.4535(3)	
O(5)	2/3	1/3	0.0689(4)	
O(6)	0.2637(3)	0.3901(3)	1/4	
O(7)	0.1764(3)	0.9745(3)	1/4	
O(8)	0.5444(3)	0.3941(3)	1/4	

[a] constrained values.

All other positions were determined from Fourier syntheses. Based on the displacement parameters, the Ba(2) atoms at the Wyckoff site 2*a* were not fully occupied. Later, the site occupation factor (SOF) for Ba(2) refined to 0.667(1). Results of the refinement of the population from powder data, 0.665(7) and 0.677(7), agree with the single crystal data (Table 2). Only a powder prepared with boric acid showed a higher population with 0.767(19). It has to be mentioned that SOF refinement from powder data has to be taken with care. In the refinement procedure, partial boron in place of aluminum occupation was considered, but this did not improve the refinement. Therefore the possible presence of boron was neglected. Tables 3 and 4 summarize atomic positional parameters and occupation and atomic displacement factors found for BAS.

The populations of Al and Si were calculated based on the refinement of the Ba occupation and interatomic distances. For Al/Si, the local occupation was determined assuming a linear behavior of the Al/Si–O bond length following Vegard's rule [10] and charge compensation. The Al(2) and Al(3) – respectively Si(2) and Si(3) – positions show the same average bond lengths of 1.714(3) Å between the coordinating oxygen atoms and the central atom. Therefore, the same SOF was assumed. The third tetrahedrally coordinated site, Al(1), has significantly larger bond lengths with an average of 1.754(3) Å.

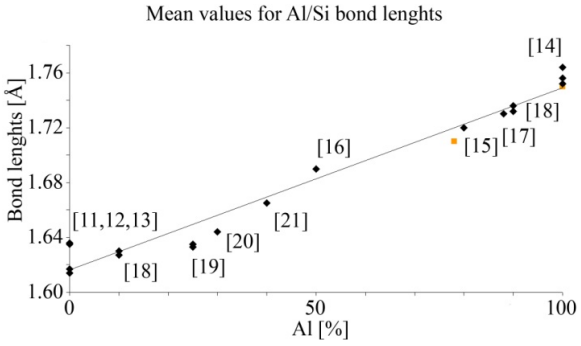

Fig. 2. Al/Si–O bond lengths in tetrahedral coordination of different aluminates and silicates. Squares mark the bond lengths of Al(1) and Al/Si(2,3) sites in the title compound.

To estimate the Al/Si ratio the data of several compounds in the literature were studied, including pure silicates and aluminates: in Ca_2SiO_4, Sr_2SiO_4 and Fe_2SiO_4 [11 – 13], the averaged Si–O bond lengths are 1.626 Å. The Al–O distances in $KAlO_2$ [14] are between 1.742 and 1.768 Å. In Fig. 2 several alkaline earth silico-aluminates and alumo-silicates with mixed Al/SiO_4 tetrahedra described in the literature are drawn *vs.* the substitution ratio. For Al/Si mixed systems, distances between 1.723 and 1.728 Å (SOF of Al $\sim$ 0.80) were found for $BaAl_2Si_2O_8$ [15], between 1.666 and 1.700 Å for $CaAl_2SiO_6$ (SOF of Al = 0.5) [16], and between 1.710 and 1.730 Å for $Sr_3Al_{10}SiO_{20}$ (SOF of Al = 0.88) [17]. These considerations have shown that the Al/Si mixed sites in BAS with bond lengths in the given range are approximately filled by 1/4 Si, and for Al(1) the site is occupied

Table 4. Atomic displacement parameters of BAS (Å^2).

	U_{11}	U_{22}	U_{33}	U_{12}	U_{13}	U_{23}
Ba(1)	0.0108(2)	0.0154(2)	0.0113(1)	0.0046(1)	0	0
Ba(2)	0.0177(3)	0.0177(3)	0.0258(5)	0.0089(2)	0	0
Ba(3)	0.0144(2)	0.0516(3)	0.0151(1)	0.0149(2)	0	0
Al(1)	0.0073(4)	0.0087(4)	0.0079(4)	0.0040(4)	0.0002(4)	−0.0003(4)
Al(2)	0.0095(4)	0.0074(4)	0.0062(4)	0.0031(4)	0.0002(4)	0.0002(4)
Si(2)	0.0095(4)	0.0074(4)	0.0062(4)	0.0031(4)	0.0002(4)	0.0002(4)
Al(3)	0.0094(4)	0.0073(4)	0.0081(4)	0.0039(4)	0.0007(4)	−0.0003(4)
Si(3)	0.0094(4)	0.0073(4)	0.0081(4)	0.0039(4)	0.0007(4)	−0.0003(4)
O(1)	0.006(1)	0.013(1)	0.023(1)	0.0025(9)	−0.001(1)	−0.0058(11)
O(2)	0.015(1)	0.015(1)	0.021(1)	0.007(1)	0.007(1)	−0.0007(11)
O(3)	0.031(1)	0.012(1)	0.014(1)	0.015(1)	−0.003(1)	−0.0007(10)
O(4)	0.012(1)	0.013(1)	0.017(1)	0.005(1)	0.0002(10)	−0.0064(11)
O(5)	0.004(1)	0.004(1)	0.010(2)	0.0023(5)	0	0
O(6)	0.027(2)	0.018(2)	0.013(2)	0.001(2)	0	0
O(7)	0.042(3)	0.017(2)	0.011(2)	0.012(2)	0	0
O(8)	0.019(2)	0.026(2)	0.008(2)	0.015(2)	0	0

Table 5. Selected bond lengths in BAS (Å).

Atom 1		Atom 2	Bond length	Atom 1		Atom 2	Bond length	Atom 1		Atom 2	Bond length
Al(1)	–	O(4)	1.725(3)	Al(2)/Si(2)	–	O(7)	1.702(2)	Al(3)/Si(3)	–	O(6)	1.700(1)
	–	O(1)	1.744(3)		–	O(3)	1.704(3)		–	O(4)	1.708(2)
	–	O(8)	1.745(2)		–	O(3)	1.720(3)		–	O(1)	1.722(3)
	–	O(5)	1.801(1)		–	O(2)	1.729(3)		–	O(2)	1.727(3)
Mean value			1.754(3)				1.714(3)				1.714(3)
Atom 1		Atom 2		Atom 1		Atom 2		Atom 1		Atom 2	
Ba(1)	–	O(3)	2.684(3)	Ba(2)	–	O(7)	2.888(4)	Ba(3)	–	O(4)	2.803(2)
	–	O(3)	2.684(3)		–	O(7)	2.888(4)		–	O(4)	2.803(2)
	–	O(6)	2.717(4)		–	O(7)	2.888(4)		–	O(2)	2.820(3)
	–	O(8)	2.790(4)		–	O(3)	3.070(3)		–	O(2)	2.820(3)
	–	O(1)	2.850(3)		–	O(3)	3.070(2)		–	O(1)	3.073(3)
	–	O(1)	2.850(3)		–	O(3)	3.070(3)		–	O(1)	3.073(3)
	–	O(2)	3.015(3)		–	O(3)	3.070(3)		–	O(8)	3.107(4)
	–	O(2)	3.015(3)		–	O(3)	3.070(2)		–	O(7)	3.405(4)
					–	O(3)	3.070(3)				

by Al only. To ensure charge neutrality, the Si substitution was fixed in the following to 22 %. Selected bond lengths of $Ba_{13.35(1)}Al_{30.7}Si_{5.3}O_{70}$ are summarized in Table 5. The Al/Si ratio was further based on the stoichiometry of the mixture of SiO_2 and $Al(OH)_3$ in the synthesis.

Further details of the crystal structure investigation may be obtained from Fachinformationszentrum Karlsruhe, 76344 Eggenstein-Leopoldshafen, Germany (fax: +49-7247-808-666; e-mail: crysdata@fiz-karlsruhe.de, http://www.fiz-informationsdienste.de/en/DB/icsd/depot_anforderung.html) on quoting the deposition number CSD-415081.

Results

Structure of $Ba_{13.35(1)}Al_{30.7}Si_{5.3}O_{70}$

The structure is built up exclusively of AlO_4 and mixed Al/SiO_4 units (Q^3) forming a three-dimensional framework of corner-sharing tetrahedra. Within this network, two types of Ba(II)-filled channels oriented along the *c* axis are found (Fig. 3). One channel includes two fully occupied Ba(II) positions, the second channel [entering in (0,0,*z*)] shows a $\sim$ 2/3 occupation by Ba(II) ions (Ba(2), Wyckoff site 2*a*). This channel is formed by 6-membered rings of corner-sharing Al/SiO_4 tetrahedra with the Ba position in the center. The tips of these tetrahedra show alternately up and down along the *c* axis and are connected *via* their corners to the next ring.

Viewed perpendicular to the *c* axis, the Ba(2) ion is located in the plane between two rings. The Ba(2) ion has a CN 6+3, 3 oxide anions coordinating within the *a,b* plane of the barium ion and 3 oxide anions above and below. The Ba–O distances to the co-planar oxide

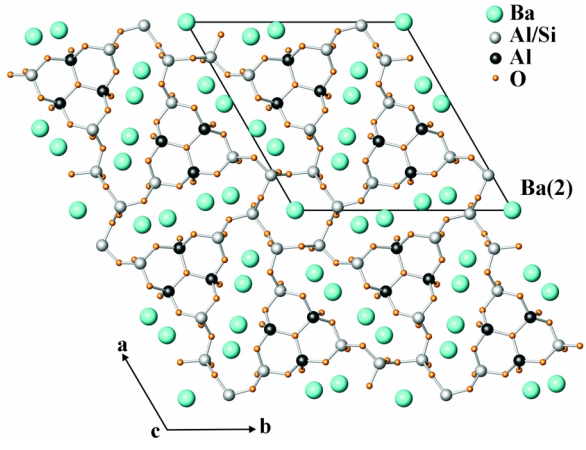

Fig. 3. Schematic drawing of the structure of BAS as seen down the crystallographic *c* axis. The drawing is cut from the [001] plane on 4 unit cells with the Ba(2) position in the center of the drawing.

anions are 2.888(4), and 3.070(3) Å to the ions above and below. Fig. 4 shows the coordination polyhedron of the Ba(2) ion.

The other channel found in this structure is filled with barium ions in two different positions, Ba(1) and Ba(3). Six channels are arranged slightly twisted counterclockwise like a propeller around a channel with the Ba(2) ions in the center. Between these channels a cluster of six corner-sharing AlO_4 tetrahedra along the *c* axis is found. The AlO_4 tetrahedra are distorted in the direction of the bridging Al–O–Al oxygen atom with a significantly larger Al–O bond length of 1.801(1) Å (typical Al–O distances in the matrix: 1.725(3)–1.745(2) Å). The O–Al–O angles range from 107.7(1) to 112.2(1)°. Mixed Al/Si tetrahedral posi-

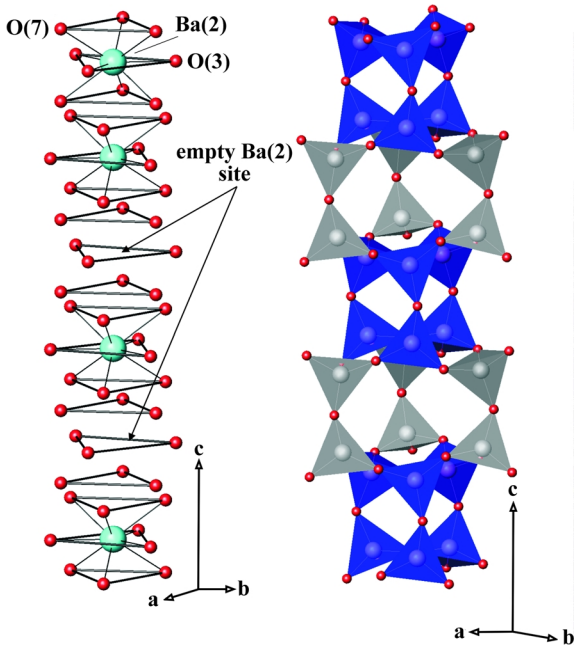

Fig. 4. Left: Possible arrangement of filled and empty sites in the disordered Ba(2) channels along the *c* axis with an SOF of $\sim 2/3$. Right: Cluster of 6 corner-bound AlO_4 tetraheda (dark grey) connected *via* 6 Al/SiO_4 tetrahedra (light grey) to the next cluster.

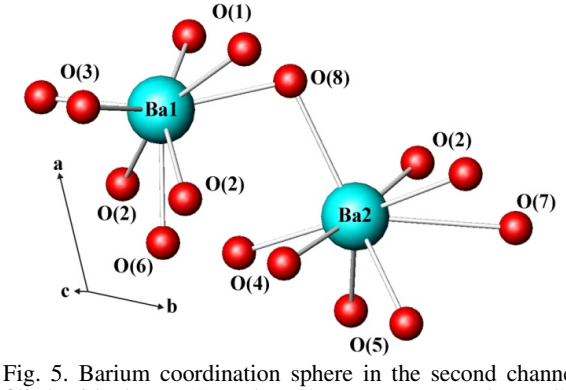

Fig. 5. Barium coordination sphere in the second channel filled with the Ba(1) and Ba(2) atoms. Ba(1) shows CN 4+2+2 and Ba(2) CN 4+3+1.

tions show ligand-central atom bond lengths between 1.700(1) and 1.729(1) Å with O–Al/Si–O angles between 105.3(2) and 113.2(2)°. Deviations from the ideal tetrahedral angle are due to coordination of the oxide anion to the barium cations. Projected perpendicular to the [001] plane, the tetrahedra form trigonal prisms adjacent to a Ba(II) channel at each side. These trigonal prisms are connected to two Al/SiO_4 tetrahedra at each corner (see Fig. 4).

The Ba(1) ion has CN 4+2+2 for the surrounding oxide anions with bond lengths between 2.684(3) and 3.015(3) Å. The Ba(3) ion shows CN 4+3+1 with bond lengths between 2.80 and 3.56 Å (see Fig. 5). At this position, 4 oxide anions are found in a planar arrangement around the center with one oxide anion above this plane [O(8)], bridging to Ba(1), and three oxide anions below.

Several Ba–O–Ba bridges can be found in this structure. The Ba(1)–O(8)–Ba(3) bridge within the rectangular channel shows bond lengths of 2.79 and 3.11 Å. A second type of oxygen bridges *via* (O(1), O(2) and O(3) have bond lengths of 2.83/3.09 Å [Ba(1)–O(1)–Ba(3)] and 3.02/2.81 Å [Ba(1)–O(2)–Ba(3)] and of 2.69 and 3.06 Å [Ba(1)–2 × O(3)–Ba(2)]. Ba(2) and Ba(3) are connected *via* O(7) with distances of 3.40 and 2.89 Å. The heavy alkaline earth ions are located in the *ab* plane perpendicular to the *c* axis with a layer distance of 4.44 Å.

Optical properties

Eu(III)-doped samples show weak red emission under UV light excitation at 254 nm and no visible emission for excitation at 366 nm. Upon reduction by hydrogen the emission properties change dramatically to a bright orange to yellow fluorescence under both wavelengths (Fig. 6). With Eu(III) completely removed, the emission spectrum is dominated by a very strong and broad band centered at *ca*. 590 nm. For the original sample, one observes 3 increasingly broad Eu(II) emission bands at *ca*. 380, 430 and 560 nm which appear to be consistent with the 3 crystallographic sites of Ba. Before reduction or with incomplete reduction one further observes bands which can

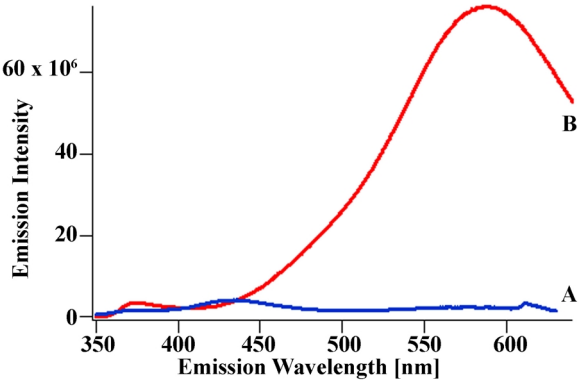

Fig. 6. Emission spectra of BAS excited at 330 nm measured before (A) and after (B) reduction.

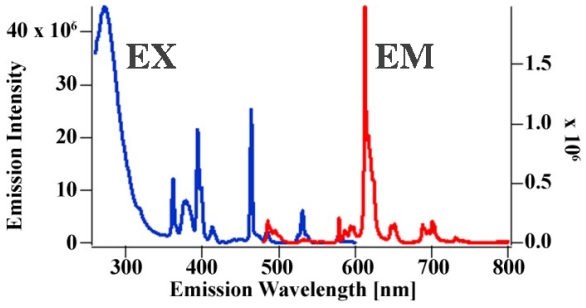

Fig. 7. Excitation spectrum (observed at 612 nm - EX) and emission spectrum (excited at 464 nm - EM) of Eu(III) in the crystal.

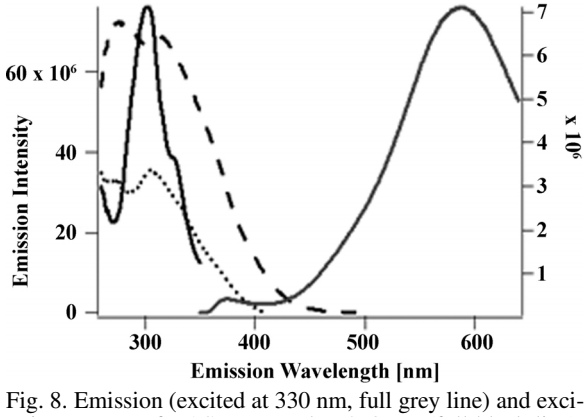

Fig. 8. Emission (excited at 330 nm, full grey line) and excitation spectra of BAS measured at 370 nm (full black line), 430 nm (dotted line) and 590 nm (dashed line).

be assigned to Eu(III). These bands can be better observed by choosing appropriate excitation and emission wavelengths, as shown in Fig. 7.

It is important to note that the emission band at 560 nm is not observed at the same position as after the reduction step (590 nm). Excitation bands (see Fig. 8) of the reduced sample at 590, 430 and 370 nm show different structures, indicating the presence of Eu(II) in different surroundings. These excitation spectra show some similarities with the corresponding excitation spectra before the reduction (see Fig. 9). In the excitation spectrum at 590 nm a new excitation line (at *ca*. 285 nm) is observed for the reduced sample.

The emission band at 560 nm (in the untreated sample) is rather strongly red-shifted compared to usual Eu(II) emission bands. Poort *et al*. have suggested for Eu(II) in $BaMgSiO_4$ that such a strong red shift may be generated by the orientation of one of the *5d* orbitals of Eu(II) due to the presence of adjacent Ba ions in a columnar stacking [22]. It is tempting to assign

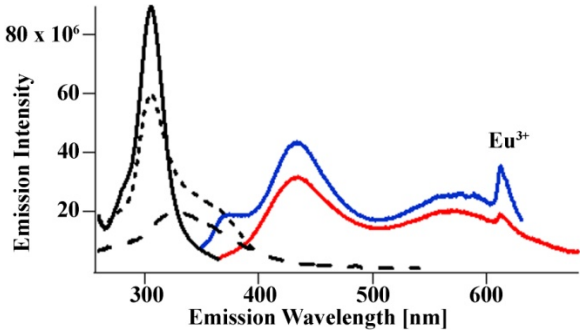

Fig. 9. Excitation and emission spectra of a BAS sample doped with 0.1 % Eu measured at 300 K: (color online) red trace: emission excited at 350 nm, blue trace excited at 330 nm; excitation spectra for the emission at 380 nm (full line), at 430 nm (dotted line) and at 560 nm (dashed line).

this band to the partially filled site with CN 6+3, but further experiments are needed to confirm this assignment. The fact that this emission band is further shifted in the reduced samples may be an indication of the possible presence of adjacent defects in the lattice. Indeed, after the reduction, Eu(III) (if it is located on a Ba site) must have some charge compensation nearby, which may not be fully removed upon reduction at 1000 °C.

Discussion

The new silico-aluminate $Ba_{13.35(1)}Al_{30.7}Si_{5.3}O_{70}$ (BAS) phase shows a channel structure with only partial occupation of Ba(2). These channels are linked by a three-dimensional network of corner-sharing Al/SiO_4 tetrahedra. Comparing lattice parameters of products of different synthetic methods suggests no boron incorporation in the structure. X-Ray measurements on different polycrystalline samples (with different mass fractions of BAS) showed similar lattice parameters and site occupation factors for Ba(2) as found from the single crystal refinement.

An unusual feature of the structure is the formation of clusters of six corner-sharing AlO_4 tetrahedra within the network, thus seemingly contradicting Loewenstein's rule [23 – 24]. This rule states, that two adjacent sites should both be occupied by Al atoms. But Loewenstein's rule imposes a certain degree of local order on the site distribution, which cannot be obtained in this Al-rich compound. Although NMR and powder diffraction studies showed an extension of this rule to Al-rich compounds, only few compounds have been found as yet with an Al–O–Al linkage [25]. The rule would be satisfied in the strictest sense if

the Al occupation results in a perfectly alternating –Al–O–Si–O–Al–O–Si– pattern (Al occupation 50 %). If this is not the case, a variation of this rule is necessary. Independent of that, a site distribution with full occupancy of the tetrahedral sites with Al ions is quite rare in alkaline earth silico-aluminates.

Doping BAS with EuF_3 leads to the incorporation of both Eu(II) and Eu(III). A total of 3 broad emission bands are observed for Eu(II), in agreement with the presence of 3 Ba sites. The overall emission intensity is rather weak. After reduction with hydrogen, the luminescence intensity increases dramatically. This new luminescence is dominated by a very broad orange-yellow emission band centered at 590 nm.

Acknowledgement

This work was supported by ETeCH Zürich and by the Swiss National Science Foundation.

[1] G. Chiari, G. Gazzoni, J. R. Craig, G. V. Gibbs, S. J. Louisnathan, *Am. Mineral*. **1985**, *70*, 969 – 974.
[2] J. V. Smith, *Acta Crystallogr*. **1953**, *6*, 613 – 620.
[3] N. P. Bansal, *J. Mater. Sci*. **1998**, *33*, 4711 – 4715.
[4] W. Gebert, *Z. Kristallogr*. **1972**, *135(5 – 6)*, 437 – 52.
[5] Y. H.Yeom, S. B. Jang, Y. Kim, S. H. Song, K. Seff, *J. Phys. Chem*. **1997**, *101*, 6914 – 6920.
[6] G. A. Novak; G. V. Gibbs, *Am. Mineral*. **1971**, *56*, 791 – 823.
[7] TOPAS 2.0, Software for Rietveld Refinement, Bruker Analytical X-ray Instruments Inc., Madison, Wisconsin (USA) **2002**.
[8] M. J. Buerger, V. Venkatakrishnan, *Proc. Nat. Acad. Sci*. **1974**, *71*, 4348 – 4351.
[9] S. D. Hall, H. D. Flack, G. M. Stewart, XTAL 3.7, Universities of Western Australia, Geneva and Maryland, **1992**.
[10] L.Vegard, *Z. Physik* **1921**, *5*, 17 – 26.
[11] H. Toraya, S. Yamazaki, *Acta Crystallogr*. **2002**, *B58*, 613 – 621.
[12] M. Catti, G. Gazzoni, G. Ivaldi, *Acta Crystallogr*. **1983**, *C39*, 29 – 34.
[13] K. Fujino, S. Sasaki, Y. Takeuchi, R. Sadanaga, *Acta Crystallogr*. **1981**, *B37*, 513 – 518.
[14] S. L. G. Hushee, J. G. Thompson, A. Melnitchenko, *J. Solid State Chem*. **1999**, *147*, 624 – 630.
[15] D. A. Griffen, P. H. Ribbe, *Am. Mineral*. **1976**, *61*, 414 – 418.
[16] F. P. Okamura, S. Ghose, H. Ohashi, *Am. Mineral*. **1974**, *59*, 549 – 557.
[17] A. Rief, F. Kubel, *Acta Crystallogr*. **2007**, *E63*, i19 – i21.
[18] G. Chiari, M. Calleri, E. Bruno, P. H. Ribbe, *Am. Mineral*. **1975**, *60*, 111 – 119.
[19] M. Gasperin, *Acta Crystallogr*. **1971**, *B27*, 854 – 855.
[20] M. J. Bennett, J. V. Smith, *Mater. Res. Bull*. **1968**, *3*, 633 – 642.
[21] J. J. Pluth, J. V. Smith, *Mater. Res. Bull*. **1972**, *7*, 1311 – 1322.
[22] S. H. M. Poort, H. M. Rejnhoudt, H. O. T. van der Kuip, G. Blasse, *J. Alloys Compd*. **1996**, *241*, 75.
[23] W. Loewenstein, *Am. Mineral* **1954**, *39*, 92.
[24] A. G. Pelmenschikov, E. A. Paukshtis, M. O. Edisherashvili, G. M. Zhidomirov, *J. Phys. Chem*. **1992**, *96*, 7051 – 7055.
[25] S. E. Dann, P. J. Mead, M. T. Weller, *Inorg. Chem*. **1996**, *35*, 1427 – 1428.